PHYSICAL REVIEW E **89**, 022407 (2014)

Crystallization in organic semiconductor thin films: A diffuse-interface approach

Alta Fang*
Department of Mechanical and Aerospace Engineering, Princeton University, Princeton, New Jersey 08544, USA

Mikko Haataja†
Department of Mechanical and Aerospace Engineering, Princeton Institute for the Science and Technology of Materials, and Program in Applied and Computational Mathematics, Princeton University, Princeton, New Jersey 08544, USA

(Received 21 November 2013; published 18 February 2014)

The crystallization of organic semiconductor thin films from an amorphous phase often results in a broad range of microstructures and molecular arrangements that in turn critically impact the electronic properties of the film. Here we present a diffuse-interface model of thin film crystallization that accounts for out-of-plane tilting of the kinetically favored crystalline orientation as well as the simultaneous appearance of multiple polymorphs. By adjusting the relative thermodynamic stability of grains oriented with the fast-growing axis either parallel or perpendicular to the substrate, crystallization can be made to occur in the form of either commonly observed spherulites or more complex morphologies such as sectors and centers. Furthermore, tuning the relative kinetic coefficients and free energies of multiple polymorphs can result in a spherulite of one crystal structure embedded within a spherulite of another crystal structure. A parametric study of the effects of anisotropy, densification, time-varying treatments, and substrate patterning reveals a wide variety of morphologies that are possible in these thin films, driven by a combination of kinetic and thermodynamics effects.

DOI: 10.1103/PhysRevE.89.022407 PACS number(s): 81.15.Aa, 68.55.−a

I. INTRODUCTION

Organic semiconductor thin films are employed in many applications such as flexible displays [1], sensors [2], and solar cells [3]. In solution-processed films, starting from an amorphous structure, nucleation processes facilitate the formation of crystalline domains [4] that significantly improve the conductivity of the films [5]. Often, kinetic frustration during the crystallization process traps organic semiconductor films into highly nonequilibrium polycrystalline states, leading to the formation of many interesting morphological features such as spherulites [6], elongated platelets [7], and feathery textures [8]. A highly complex relationship exists between the processing methods used to fabricate the film and its final morphology since intermolecular and intramolecular interactions with the substrate and solvent play a role in determining the structural organization of the film [9,10]. Molecular orientation strongly influences the electrical mobility of organic semiconductor films [11,12] and can also affect optical absorption [13], while grain boundaries and film morphology can have a strong impact on charge transport processes [14–16]. A better understanding of the physical mechanisms that lead organic semiconductor thin films to crystallize in different molecular orientations and microstructures as well as greater knowledge of the relationship between these two characteristics are thus crucial for improved control of material and device properties.

Existing models of crystallization and microstructure formation in thin films have been able to simulate a wide range of morphologies [17,18], but in these models the molecular stacking directions have been confined to the two-dimensional (2D) plane of the film. It has been shown experimentally, however, that postdeposition processing can induce amorphously deposited films of organic molecules [such as contorted hexabenzocoronene (HBC)] to crystallize preferentially in distinct out-of-plane orientations, including configurations where the molecular π-stacking direction is nearly perpendicular to the plane of the film [8].

In this work we introduce a diffuse-interface model to study crystal growth in thin films of anisotropic molecules whose fast-crystallizing axis is allowed to take on any orientation, including those tilted out of the plane of the film. We use a continuum model to focus on the structure of the film on length scales of tens to hundreds of microns. Since several organic semiconductors exhibit a preference for crystallizing with π planes stacking either parallel or perpendicular to the substrate [8,19–21], we introduce a free energy that can be tuned to adjust whether either or both of these configurations are thermodynamically favored. In addition, given that the film thicknesses in experiments are typically on the order of $\sim$100 nm [6,8,12], growth will be constrained to two dimensions. Thus, rather than explore the morphologies of fully 3D spherulites as has been done previously [22,23], herein we study the physics of phase transitions on a 3D free energy landscape with only a 2D space in which growth is permitted. Furthermore, experimental evidence suggests that by annealing films of contorted HBC with certain solvent vapors, multiple polymorphs can appear simultaneously in the same film [24] and polymorphism is in fact displayed by many other organic semiconductors as well [25]. Therefore, the model allows the free energies and mobilities of each polymorph to be independently tuned since an interplay between both thermodynamic and kinetic effects is important for the formation of concomitant polymorphs [26].

Our parametric simulation study reveals that complex morphologies (such as sectors and centers) emerge when certain regions of the film crystallize in one of the thermodynamically favored out-of-plane orientations while others

*alta@princeton.edu
†mhaataja@princeton.edu

crystallize in the other orientation as a result of either (i) nucleating growth with differently oriented initial seeds, (ii) applying time-varying treatments, or (iii) patterning the substrate. Further diversity of microstructure was achieved by changing the degree of densification, which leads to branched structures, and introducing multiple polymorphs, which can lead to embedded spherulites. In broader terms, the modeling approach and results reported herein form the basis for a more quantitative study of nucleation and growth processes in organic semiconductor thin film systems.

The rest of the paper is organized as follows. In Sec. II we outline the diffuse-interface framework employed in this work. Then, results from our simulation studies and their implications are discussed in Sec. III. Finally, a brief summary and concluding remarks are presented in Sec. IV.

II. MODEL

Our model builds on previous vector-valued diffuse-interface models for polycrystalline solidification [27–31]. More specifically, we use a 3D vector order parameter $\vec{\phi}_i$ for each polymorph, indexed by i. The magnitude of $\vec{\phi}_i$ represents the degree of crystallinity such that $|\vec{\phi}_i| = 1$ (0) corresponds to the crystalline (amorphous) phase. The direction of $\vec{\phi}_i$ in turn represents the axis of fast crystal growth, which, in the case of molecules with aromatic rings such as contorted HBC, corresponds to the direction of π stacking [see Fig. 1(a)]. Although a complete description of a 3D orientation requires an additional variable to track rotations in the plane perpendicular to $\vec{\phi}$, here we assume the value of this rotational angle to be constant throughout the film, which makes the model significantly simpler than a full treatment of 3D polycrystallinity using quaternions [22,23] or orthogonal matrices [32]. Further discussion of advantages and disadvantages of these different modeling frameworks is presented in Sec. IV.

In addition, branched morphologies in some experimentally observed thin films suggest that crystal growth can be diffusion limited. In particular, since branching can occur even in single-component films, it may be a result of densification (rather than redistribution of impurities in multicomponent systems), which can lead to the depletion of available molecules ahead of the growth front and the subsequent formation of dendritic morphologies. To account for such effects phenomenologically, we introduce a conserved scalar order parameter $u(\vec{r},t)$ that is analogous to the dimensionless undercooling in solidification processes [31] and can be directly related to the effective densification factor, as will be discussed in further detail following Eq. (9).

The free energy functional includes both interfacial energy terms and a bulk free energy term for each of the N_p polymorphs, as well as a coupling term that penalizes the presence of multiple polymorphs at the same location:

$$F = \sum_{i=1}^{N_p} \int d\vec{r} \left(\frac{\epsilon_i^2}{2} [(\vec{\nabla}\cdot\vec{\phi}_i)^2 + |\vec{\nabla}\times\vec{\phi}_i|^2] + f_i(\vec{\phi}_i,u) + a \sum_{j=i+1}^{N_p} |\vec{\phi}_i|^2 |\vec{\phi}_j|^2 \right), \tag{1}$$

where

$$f_i(\vec{\phi},u) = \frac{1+b_1\cos(n\theta)\sin^2\varphi}{4(1+b_1)} \frac{1+b_2\cos(4\varphi)}{1+b_2} |\vec{\phi}|^4 + \frac{m_i(u) - \frac{3}{2} - \widetilde{\lambda}_i\cos^2\varphi}{3} |\vec{\phi}|^3 - \frac{m_i(u) - \frac{1}{2} - \widetilde{\lambda}_i\cos^2\varphi}{2} |\vec{\phi}|^2, \tag{2}$$

$$m_i(u) = \frac{\alpha_i}{\pi} \tan^{-1}(-\gamma u), \tag{3}$$

and

$$\widetilde{\lambda}_i = \lambda_i + \frac{3b_1}{2(1+b_1)}, \tag{4}$$

with the following constraints on parameter values:

$$0 < \alpha_i < 1, \quad -\frac{1}{2} + \frac{3b_1}{1+b_1} + |\widetilde{\lambda}_i| < m_i < \frac{1}{2} - |\widetilde{\lambda}_i|, \quad -1 < b_2 < 0. \tag{5}$$

We have defined φ as the angle between $\vec{\phi}$ and the z axis, so $\varphi = 90^\circ$ represents the edge-on orientation with the edges of the π planes pointing into the substrate, while $\varphi = 0^\circ$ represents the face-on orientation with the faces of the π planes parallel to the substrate. (Note that we have dropped the i subscripts since this discussion applies to all polymorphs.) Furthermore, θ denotes the angle between the x axis and the projection of $\vec{\phi}$ onto the x-y plane. The constraints in Eq. (5) ensure that $|\vec{\phi}| = 0$ and 1 as well as $\varphi = 0^\circ$ and 90° are always local minima of f.

The bulk free energy f is constructed to have a double-well shape in both $|\vec{\phi}|$ and φ, with m and λ dictating the relative depths of the local minima. This form of the bulk free energy reflects the existence of a first-order phase transition between the amorphous and crystalline phases, while we use a similarly shaped potential in the tilt angle φ [see Figs. 1(b) and 1(c)], as the edge-on and face-on configurations are commonly observed experimentally and represent the limiting cases for possible out-of-plane orientations. Physically, we envision that m and λ can be varied, for example, by altering the substrate, exposing the surface of the film to different substances, or heating the film. The parameter b_2 dictates the height of the free energy barrier between the $\varphi = 0^\circ$ and 90° orientations, while Eq. (4) ensures that the values of f at these minima are equal when $\lambda = 0$. Finally, grain boundaries are stabilized by introducing a θ dependence in f such that certain in-plane orientations are preferred, allowing fixed misorientations to exist [see Fig. 1(d)]. The parameter b_1 dictates the depth of these equispaced local free energy minima, while n controls the number of such minima.

Given the free energy in Eq. (1), the time evolution of $\vec{\phi}_i$ and u is computed in Cartesian coordinates as follows:

$$\frac{\partial\phi_{ix}}{\partial t} = -M_i \frac{\delta F}{\delta\phi_{ix}} + \eta_{ix}, \tag{6}$$

$$\frac{\partial\phi_{iy}}{\partial t} = -M_i \frac{\delta F}{\delta\phi_{iy}} + \eta_{iy}, \tag{7}$$

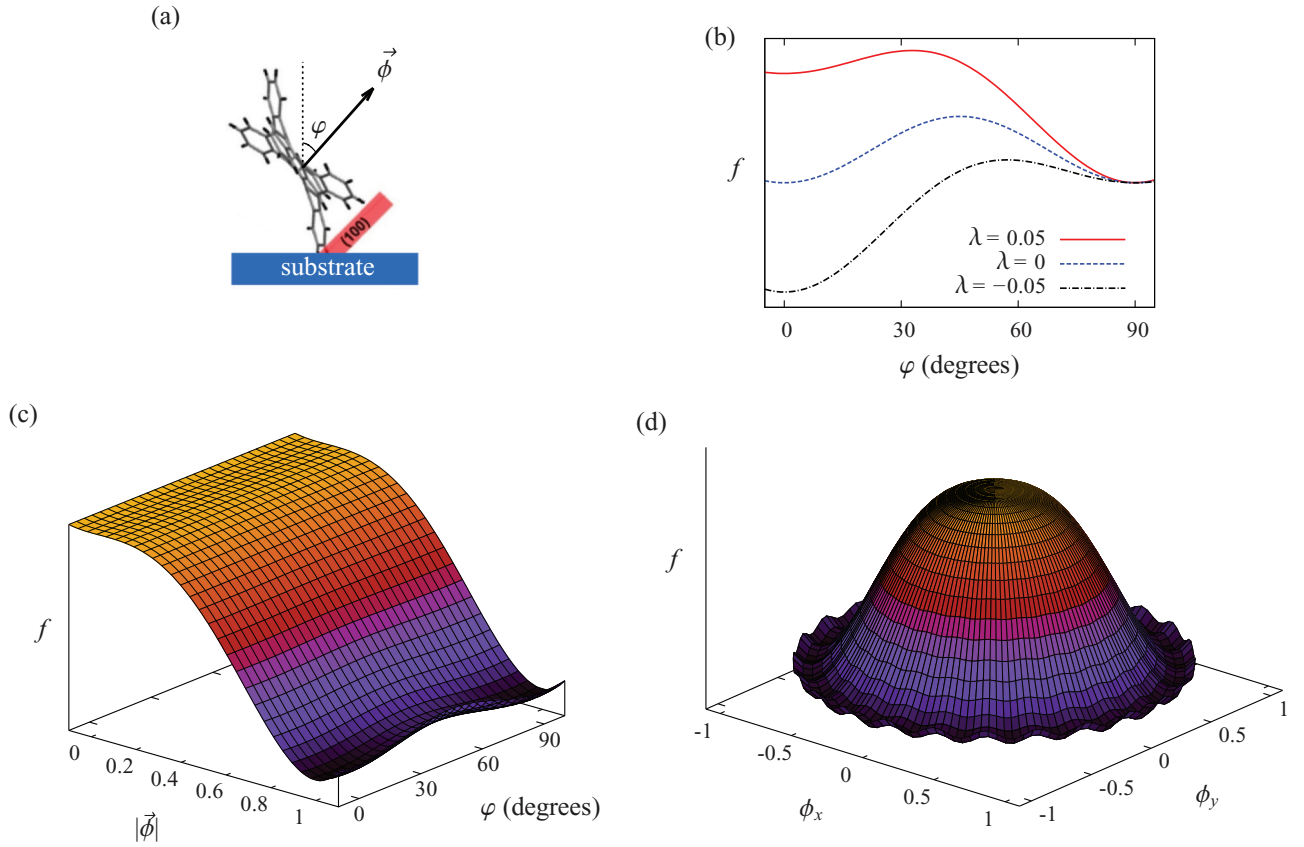

FIG. 1. (Color online) (a) Schematic adapted from Ref. [8] showing that $\vec{\phi}$ is oriented along the molecular π-stacking direction and tilted at an angle φ with respect to the z axis. (b) Parameter λ can be tuned to vary the relative free energies of the two preferred out-of-plane orientations. (c) The free energy has local minima in both $|\vec{\phi}|$ and φ, shown here for $\theta = 0^\circ$, $m = 0.42$, and $\lambda = 0$. Note the presence of a rather shallow well at $|\vec{\phi}| = 0$ and a much deeper one at $|\vec{\phi}| = 1$. (d) To incorporate multiple crystalline orientations, n equispaced values of the in-plane orientation θ are singled out by f, as demonstrated for $\varphi = 90^\circ$, $m = 0.42$, $\lambda = 0$, and $b_1 = -0.005$.

$$\frac{\partial \phi_{iz}}{\partial t} = -M_i \frac{\delta F}{\delta \phi_{iz}} + \eta_{iz}, \tag{8}$$

$$\frac{\partial u}{\partial t} = \nabla^2 u + \sum_{i=1}^{N_p} \frac{1}{\Delta_i} \frac{\partial |\vec{\phi}_i|}{\partial t}. \tag{9}$$

Here Δ is a tunable parameter that is related to the degree of densification during crystallization and thus controls how diffusion limited the crystal growth is. In particular, $\Delta \gg 1$ ($\Delta \to 0$) corresponds to low (high) degree of densification. More specifically, given the boundary conditions employed in the simulations, for $\Delta < 1$, a fraction Δ of the system will crystallize before the effective supercooling is depleted. Thus, the magnitude of Δ is physically determined by $\Delta = \rho_{\text{amorph}}/\rho_{\text{cryst}}$, where $\rho_{\text{amorph}}/\rho_{\text{cryst}}$ is the densification factor and ρ_i denotes the effective areal density of the ith phase. The field m is in turn coupled to the conserved field u via Eq. (3) such that as the conserved quantity is depleted, the driving force for crystallization disappears. Furthermore, the following form for the mobility is used:

$$M = \widetilde{M}\{1 + \delta_\theta(1 + \cos[2(\psi - \theta)])\sin^2\varphi\}[1 + \delta_\beta(1 + \cos(k\psi))\cos^2\varphi], \tag{10}$$

where

$$\widetilde{M} = \frac{M_{\max} g(|\vec{\phi}|)}{1 + 2\delta_\theta},$$

$$g(|\vec{\phi}|) = \frac{1}{2}\left[1 + \tanh\left(-\frac{|\vec{\phi}| - \bar{c}}{\tilde{c}}\right)\right],$$

$$\psi = \tan^{-1}\left(\frac{\partial|\vec{\phi}|}{\partial y} \Big/ \frac{\partial|\vec{\phi}|}{\partial x}\right),$$

and $\delta_\theta > \delta_\beta > 0$. Here ψ denotes the local orientation of the growth front. Because no coarsening is observed experimentally, the mobility is modulated such that its value is orders of magnitude smaller in crystalline regions than in amorphous regions, effectively freezing the film in a kinetically trapped state [see Fig. 2(a)]. In particular, $\bar{c}$ is the threshold value of $|\vec{\phi}|$ above which the mobility approaches zero, while $\tilde{c}$ dictates the range of $|\vec{\phi}|$ values over which this transition in mobility occurs. Furthermore, the mobility used here has a twofold-symmetric anisotropy δ_θ in the fast-growing crystallographic axis because it has been found that in many organic small-molecule systems with planar geometries, the direction of the crystal growth is aligned with the one associated with π stacking [6]. Thus, when the molecules are oriented edge-on, the mobility is at a maximum ($M = M_{\max}$) if the projection of

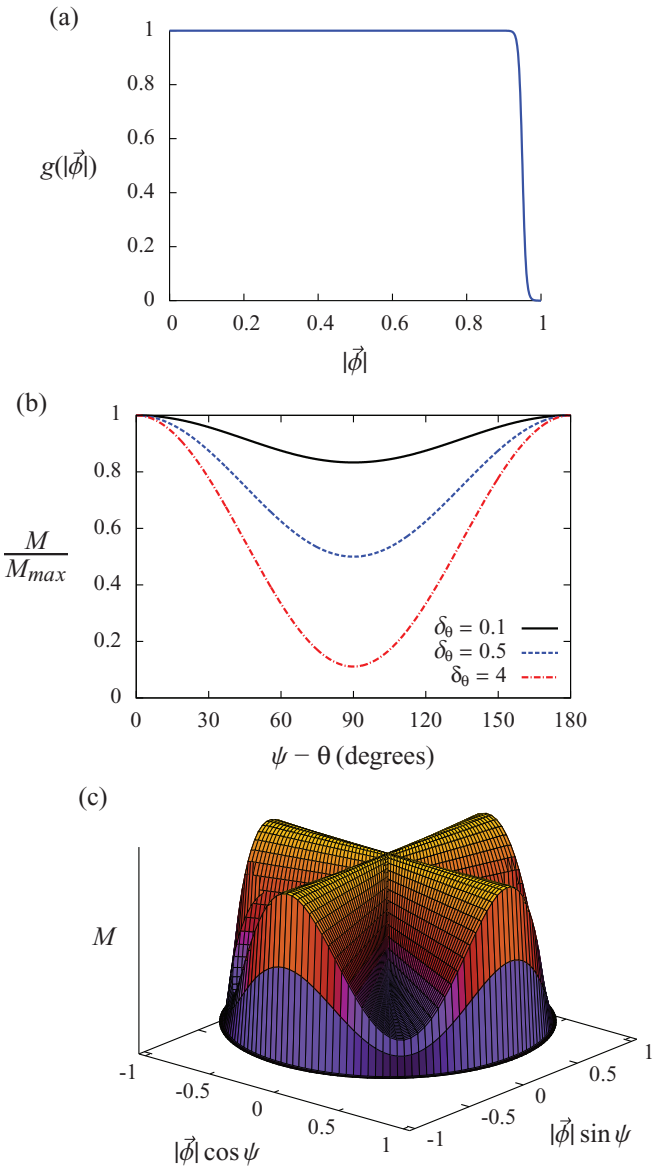

FIG. 2. (Color online) (a) The mobility M effectively vanishes as $|\vec{\phi}| \to 1$, thereby freezing the order parameter $\vec{\phi}$ in the crystalline phase. (b) Edge-on orientations, corresponding to $\varphi = 90^\circ$, experience an anisotropic mobility that is at a maximum when the growth direction ψ is aligned with the in-plane orientation θ and at a minimum when they are perpendicular. (c) Face-on orientations, for which $\varphi = 0^\circ$, can also be made to have an anisotropic mobility, as demonstrated here for $k = 4$ and $\delta_\beta = 2$. The mobility attains a maximum for four growth directions ψ and decreases sharply for all values of ψ as $|\vec{\phi}| \to 1$.

$\vec{\phi}$ onto the x-y plane is parallel to the crystal growth direction and at a minimum if they are perpendicular [see Fig. 2(b)]. In the face-on case, anisotropy in the crystallographic directions perpendicular to $\vec{\phi}$ can be controlled by adjusting δ_β, which controls the magnitude of the k-fold anisotropy, as illustrated in Fig. 2(c). The factors of $\sin^2\varphi$ and $\cos^2\varphi$ in Eq. (10) ensure that when a region of the film has an edge-on orientation, the anisotropy is dictated by δ_θ, while face-on regions instead have a k-fold symmetric anisotropy δ_β in the plane of the thin film.

Finally, stochastic fluctuations are introduced through η, which obey

$$\langle \eta(\vec{r},t)\rangle = 0, \quad \langle \eta(\vec{r},t)\eta(\vec{r}\,',t')\rangle = \tilde{\eta}^2 R(\vec{r},\vec{r}\,';l)\delta(t-t'), \quad (11)$$

where

$$R(\vec{r},\vec{r}\,';l) = \frac{1}{2\pi l^2}\exp\left(\frac{-|\vec{r}-\vec{r}\,'|^2}{2l^2}\right) \quad (12)$$

and

$$\tilde{\eta} = 4|\vec{\phi}|(1-|\vec{\phi}|)\sqrt{2k_B T M_{\max} g(|\vec{\phi}|)}. \quad (13)$$

The presence of time-varying fluctuations at the interface is essential to accurately simulating spherulites since their polycrystallinity arises from growth front nucleation [17]. Here we do not use the usual uncorrelated Gaussian noise but instead use fluctuations that are spatially correlated over a length scale l. Physically, this reflects the fact that the initial supposedly amorphous films are often not completely disordered but have small regions with distinct orientations [6]. Furthermore, the noise is modulated to allow fluctuations to occur only at the interface and not in either the fully amorphous or crystalline phases. This prevents nucleation from happening in the amorphous phase so that the morphologies of the crystalline domains can be more clearly discerned.

To study the morphologies that arise from this model using numerical simulations, initially a small seed with out-of-plane orientation φ_0 is placed in the center of a square simulation grid with periodic boundary conditions and the time evolution of the system is computed with explicit finite-difference methods. A nine-point stencil for the Laplacian is used to reduce grid anisotropy artifacts and Fourier transforms are used to generate the spatially correlated noise [33]. Representative nondimensionalized parameter values used are $N_x = N_y = 1024$, $\Delta t = 2.4 \times 10^{-5}$, $M_{\max} = \frac{5}{3} \times 10^4$, $\Delta x = 0.01$, $\epsilon^2 = 10^{-5}$, $n = 24$, $l^2 = 10^{-5}$, $b_1 = -0.0025$, $b_2 = -0.01$, $\alpha = 0.9$, $\gamma = 10$, $k_B T = 1.2 \times 10^{-8}$, $\bar{c} = 0.95$, $\tilde{c} = 0.01$, and $a = 0.5$. Numerical implementation of this model faces the challenge that numerical artifacts may arise if interfaces are resolved by too few grid points, but physical interfacial widths are extremely small and fine grids are computationally expensive. Therefore, in these simulations we use an interface width that is larger than what is physical, while carefully choosing parameter values that lead to physically reasonable results.

III. RESULTS

We begin our exploration of the model by considering the effects of the parameters λ and Δ, which account for the thermodynamic preference of edge-on vs face-on configurations and densification effects, respectively, on crystalline morphologies. In all simulations reported below, unless otherwise stated, we only consider one polymorph and set $N_p = 1$. To this end, Fig. 3 illustrates some of the crystallization patterns that can form for various values of λ and Δ in the cases of both low- and high-mobility anisotropy. Since experimentally spherulites are often visualized using polarized optical micrographs where color indicates the local orientation, here we use a cyclic color map to visualize θ and show

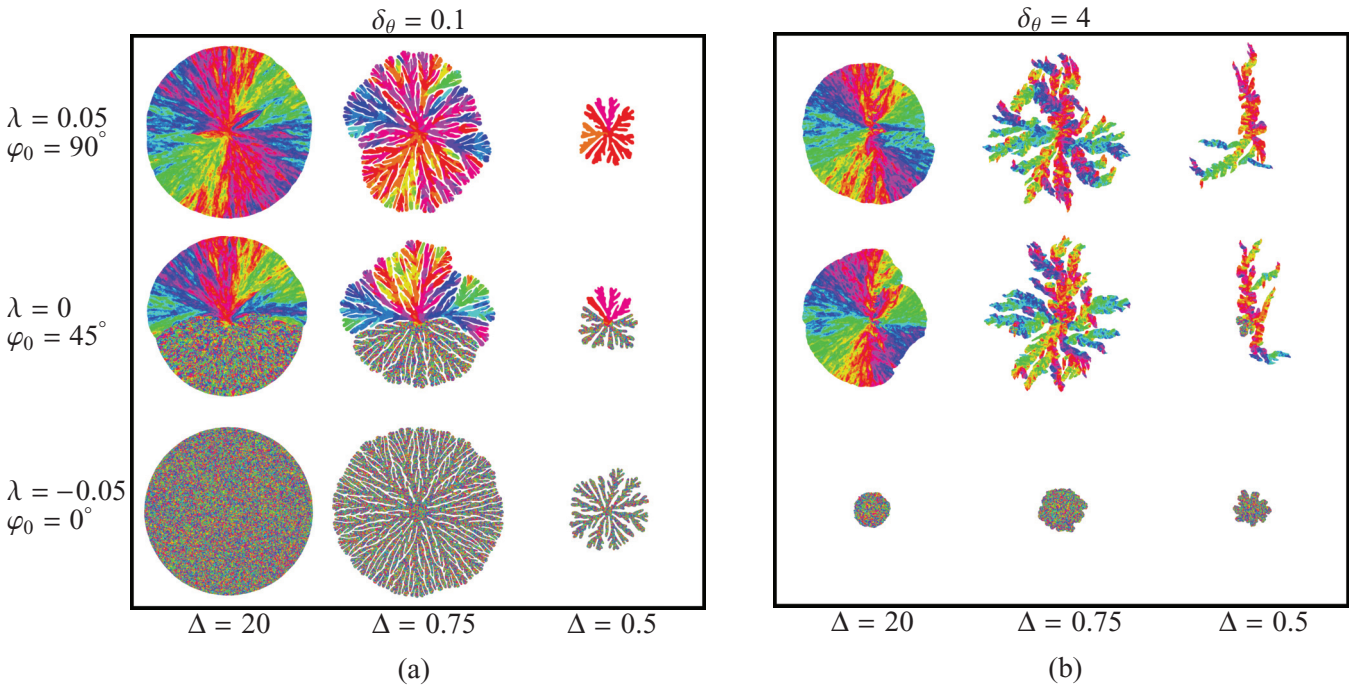

FIG. 3. (Color online) Representative morphologies from simulations with (a) a relatively low mobility anisotropy $\delta_\theta = 0.1$ and (b) a relatively high mobility anisotropy $\delta_\theta = 4$, taken at 7000, 12 000, and 14 000 time steps (left to right in each panel). Colors represent θ, the crystalline orientation projected onto the x-y plane, with angles differing by 180° considered equivalent. As the bulk free energy landscape is changed by varying λ from 0.05 to 0 to -0.05 and the initial seed orientation φ_0 is varied from 90° to 45° to 0° (top to bottom), the film crystallizes with all edge-on, sectors of edge-on and face-on, or all face-on orientations, respectively, for a low anisotropy of $\delta_\theta = 0.1$. Note that for high-δ_θ values, sector morphologies consisting of coexisting regions of edge-on and face-on orientations are no longer observed for the case of $\lambda = 0$, as the edge-on configurations quickly outgrow the face-on ones. Also note that decreasing Δ leads to more branched morphologies, as expected.

uncrystallized regions in white. We accurately reproduce commonly observed thin film spherulites by using an initial seed with $\varphi_0 = 90^\circ$ and letting $\lambda > 0$, which causes the bulk free energy to favor crystallization in an edge-on orientation.

Novel microstructures can arise when we let $\lambda = 0$, which causes both edge-on and face-on orientations to have the same free energy, and we use an initial seed with $\varphi_0 = 45^\circ$, which is an unstable state exactly between the two preferred orientations. The bulk free energy causes sector-shaped morphologies to arise for low mobility anisotropy values, as fluctuations drive some regions (sectors) of the spherulite to crystallize in the edge-on configuration and others to crystallize face-on. The intermediately oriented initial seed is crucial for the formation of these sectors since an initial seed of edge-on orientation would simply result in a fully-edge-on spherulite while a face-on seed would result in a face-on center that transitions to edge-on crystallization for kinetic reasons, as described in more detail below. Interestingly, for high-δ_θ values, sectors are no longer observed for the case of $\lambda = 0$, as the edge-on configurations quickly outgrow the face-on ones. Finally, when $\lambda < 0$ and $\varphi_0 = 0^\circ$, the film crystallizes in an entirely face-on alignment. We note that the projection of $\vec{\phi}$ onto the x-y plane appears speckled due to small frozen-in fluctuations that slightly tilt the vector away from the vertical.

With regard to the role of densification, decreasing Δ is accompanied by a morphological transition from compact spherulites to branched structures with increasing amounts of amorphous material trapped between the crystallized regions. In the case of low anisotropy, these branched structures appear seaweedlike in shape with rounded edges and an overall circular growth habit as expected, while for the case of high anisotropy, the branch tips are sharply pointed with more widely separated and meandering dendritic arms. Additionally, decreasing Δ also slows down the rate of crystallization. For a high level of anisotropy and in the limit of very low noise amplitude, elongated needles form at all values of Δ.

It should be noted that in Fig. 3, the face-on crystal grows in a circular shape because we set $\delta_\beta = 0$ so that the crystal is rotationally invariant in the plane perpendicular to $\vec{\phi}$. Anisotropy in that plane can be introduced through nonzero values of δ_β and k, as shown in Fig. 4. Faceted face-on crystals grow when there is a low level of densification, while dendritic structures form when the effect of densification is stronger. In particular, the magnitude of δ_β dictates the difference in the rate of crystallization between the fast and slow axes, so a higher value of δ_β leads to sharper corners in the faceted case and sharper needles in the dendritic case.

From these simulations, histograms of out-of-plane orientation values for the crystallized regions can be extracted as shown in Fig. 5. As expected, the peaks in the distributions correspond to edge-on and face-on orientations since the double-well potential in φ explicitly discourages crystallization in intermediate orientations. The width of the peaks increases with larger noise amplitudes, as larger fluctuations

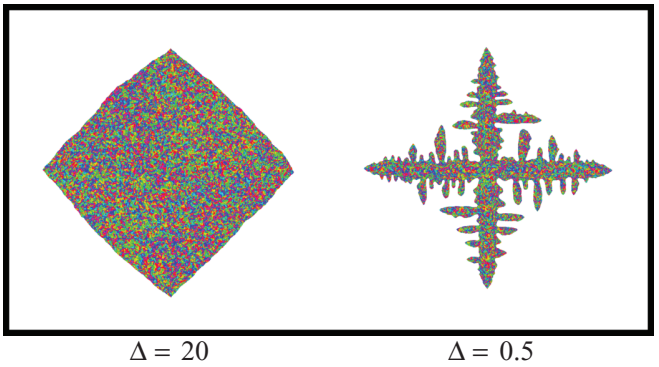

FIG. 4. (Color online) When anisotropy is introduced in the plane perpendicular to $\vec{\phi}$ by setting $k = 4$ and $\delta_\beta = 2$, a fourfold symmetric face-on crystal forms for $\lambda = -0.05$ and $\varphi_0 = 0^\circ$. When $\Delta = 20$ the shape is faceted, while when $\Delta = 0.5$ the shape is dendritic.

in φ become subsumed into the crystal growth front. The drop in normalized frequency near $\varphi = 0^\circ$ that results in the face-on maxima being shifted slightly away from $\varphi = 0^\circ$ is due to the fact that a histogram of φ values is a measure of the *polar* probability distribution rather than a probability density function. That is, even though a probability density function $p(\varphi)$ may have a maximum at $\varphi = 0^\circ$ [and in fact does, as per f_i in Eq. (2)], the probability of finding an out-of-plane orientation in the interval from φ to $\varphi + \Delta\varphi$ is given by $\Pr(\varphi, \varphi + \Delta\varphi) \propto p(\varphi) \sin\varphi \Delta\varphi$, so the factor of $\sin\varphi$ will always cause the polar probability distribution to approach 0 as $\varphi \to 0^\circ$ for finite $p(\varphi)$.

We note that these orientation distributions can be compared with intensity profiles of particular crystalline plane reflections in experimental grazing-incidence x-ray-diffraction (GIXD) data. Care must be exercised with direct comparisons, however, as kinetic effects may suppress or enhance the frequency of occurrence of certain orientations. For example, in the case of high mobility anisotropy values, edge-on configurations quickly outgrow the face-on ones and effectively eliminate them from the orientation distribution, even though both configurations are equally stable thermodynamically for $\lambda = 0$. Nevertheless, in conjunction with kinetic data, the GIXD data can be employed to constrain the number of thermodynamically favored orientations.

Additional intriguing microstructures arise when the bulk free energy is suddenly changed during the crystallization process, which physically corresponds to applying time-varying treatments to the film. Figure 6 shows that centers with a different out-of-plane orientation than their neighboring outer ring form when crystallization is first begun with $\lambda > 0$, which favors edge-on orientations, and then after some time the bulk free energy is switched to favor face-on orientations by setting $\lambda < 0$ or vice versa. The jagged interface at the transition between the two regions in such center morphologies in Fig. 6 reflects the fact that the change in orientations is driven by fluctuations that cause different parts of the interface to overcome the energy barrier and transition from the metastable to the stable state at different times. Indeed, the transition between a center of one orientation and its surrounding crystal of a different orientation can take on different geometries depending on the energetics and kinetics of the film, as we will discuss next.

Now, the top row of Fig. 7 shows the morphology that arises when both the edge-on and face-on orientations have the same free energy, but edge-on crystals grow twice as fast as face-on crystals and the initial seed is face-on. Faster-growing edge-on grains nucleate at various points along the interface and eventually pinch off the face-on growth front, resulting

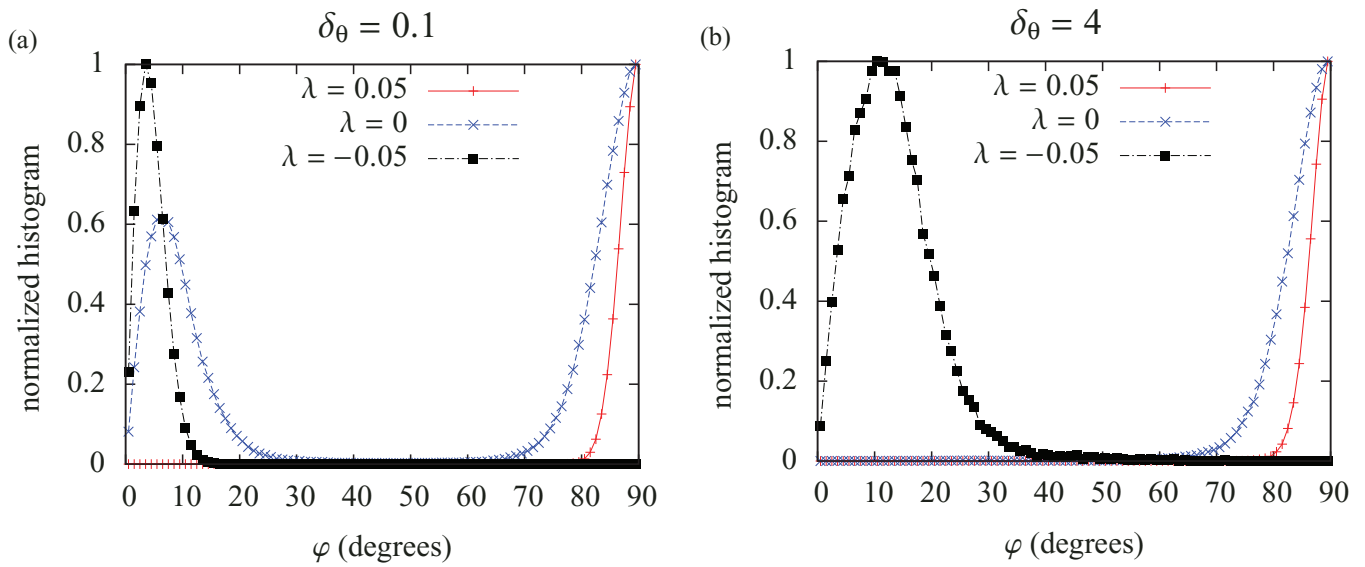

FIG. 5. (Color online) Histograms of out-of-plane orientations for crystallized regions of the structures with (a) a low and (b) a high value of the mobility anisotropy δ_θ, for $\Delta = 20$. The film crystallizes in primarily edge-on, primarily face-on, or a combination of both orientations as dictated by the value of λ. Note that for high δ_θ and $\lambda = 0$, edge-on configurations quickly outgrow the face-on ones and effectively eliminate them from the orientation distribution, even though both configurations are equally stable thermodynamically.

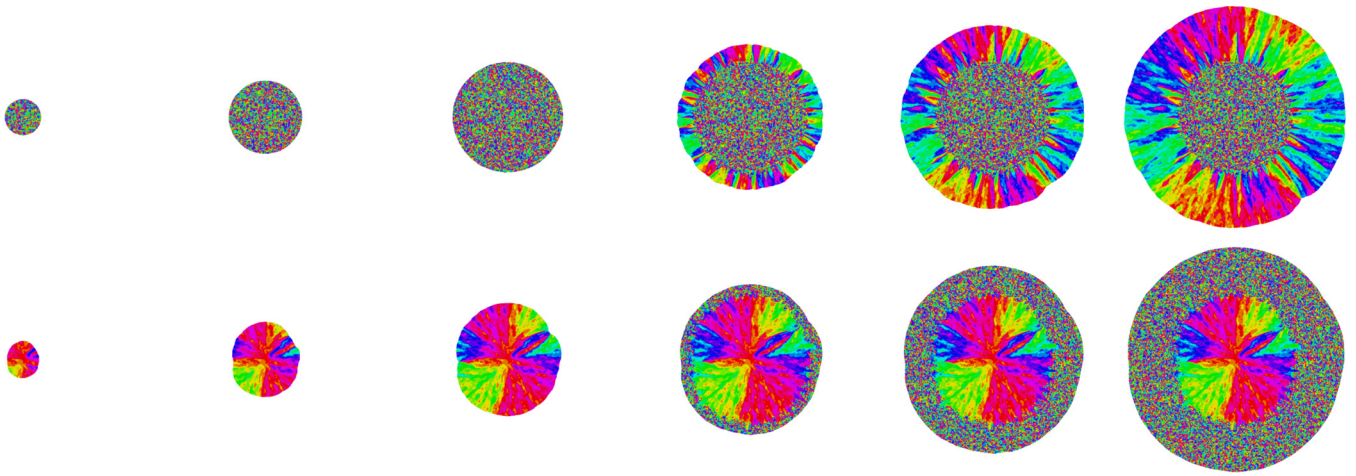

FIG. 6. (Color online) Simulated configurations shown every 1200 time steps during crystallization. The parameter λ was changed from -0.05 to 0.05 (top row) or 0.05 to -0.05 (bottom row) after 3600 time steps. This change causes the film that began crystallizing face-on to subsequently switch to crystallizing edge-on, or vice versa. Here a low value for the mobility anisotropy ($\delta_\theta = 0.1$) was used.

in a flower-petal shape. Such patterns have been observed experimentally in polyhydroxybutyrate [34]. In the bottom row of Fig. 7, a time-varying treatment identical to that in the bottom row of Fig. 6 was applied to a system with a higher anisotropy of $\delta_\theta = 0.5$. Note the presence of narrow strands of edge-on crystals at the interface, which arise because edge-on crystallization proceeds faster than face-on crystallization, resulting in the rapid growth of the edge-on crystals radially outward from the seed crystal until the transition to the lower-energy face-on orientation takes place.

If the substrate is patterned so that certain regions favor crystallization in the edge-on orientation while others favor the face-on orientation, arbitrarily shaped regions of different orientation can be created. An example is shown in Fig. 8, where $\lambda = -0.05$ within a square ring while $\lambda = 0.05$ everywhere else. The initial edge-on crystal seed grows radially outward, switches to the face-on orientation in the region inside the square ring, and then switches back to the edge-on orientation again. Inequalities in the mobilities of the two orientations and the need to overcome the energy barrier to the favored orientation through fluctuations introduces roughness to the interface and a lag in transitioning between orientations. The resolution of the features achievable from substrate patterning thus can be limited by these considerations.

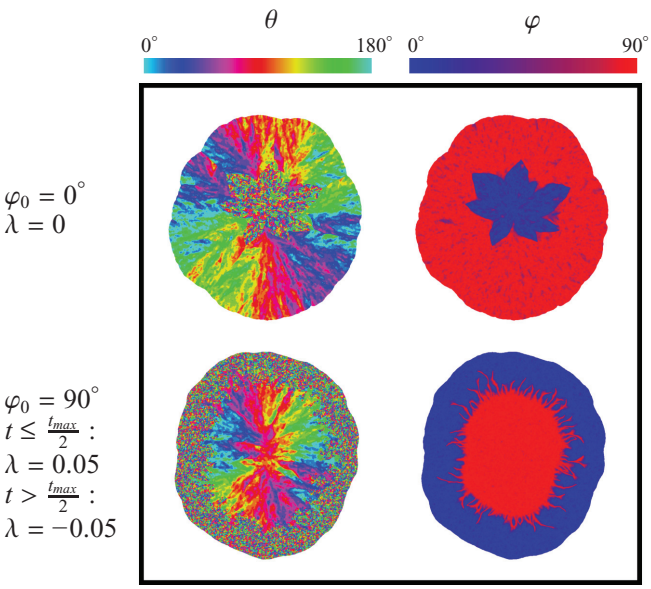

FIG. 7. (Color online) When edge-on crystallization is faster than face-on crystallization and a face-on initial seed is used, a flower-petal-shaped center arises as the faster-growing orientation pinches off the slower-growing orientation (top row). In contrast, when a time-varying treatment energetically favors a transition from the edge-on to the face-on orientation, strands of the faster-growing edge-on orientation persist for some time before switching to the lower-energy state (bottom row). An intermediate value for the mobility anisotropy ($\delta_\theta = 0.5$) was used for both simulations.

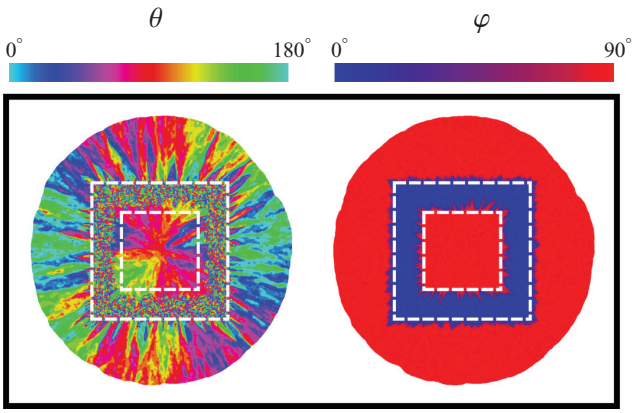

FIG. 8. (Color online) When the substrate is patterned such that $\lambda = -0.05$ inside a square ring (indicated by dashed white lines) while $\lambda = 0.05$ everywhere else, crystallization proceeds in the locally energetically favored orientation, with jagged edges where transitions between preferred molecular orientations have occurred. Here $\delta_\theta = 0.1$.

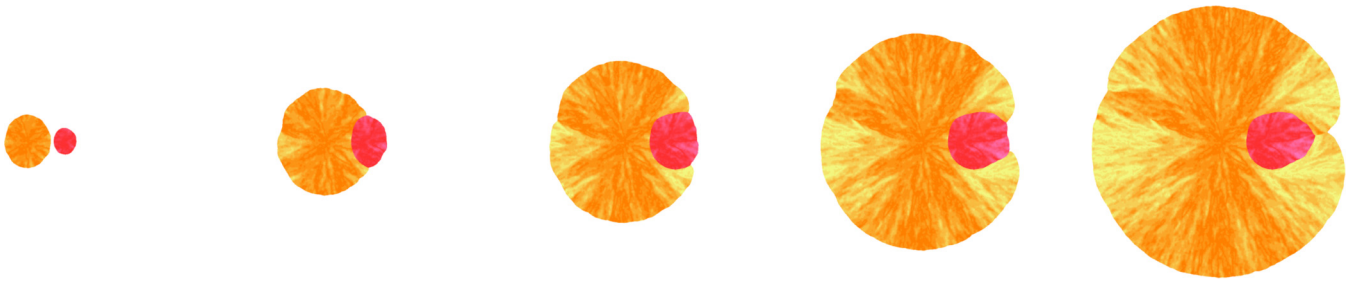

FIG. 9. (Color online) Snapshots at $t = 1400$, 2800, 4200, 5600, and 7000 (left to right) time steps show a spherulite of one polymorph becoming embedded within a spherulite of another, faster growing polymorph. Shades of red (dark) represent θ for the lower-mobility polymorph and shades of orange (light) represent θ for the higher-mobility polymorph.

Finally, when multiple polymorphs crystallize in the same thin film, an even greater variety of microstructures is possible. Arbitrarily many polymorphs can be simulated with our model by using an additional vector order parameter field $\vec{\phi}_i$ to track the evolution of each polymorph. To demonstrate this, we simulate two polymorphs with the same free energy but different crystallization rates. When an initial seed of each polymorph is placed in the film with $\alpha_1 = \alpha_2 = 0.9$ so that both equally favor a transition to the crystalline state and $M_{1,\max} = 2M_{2,\max}$ so that one polymorph crystallizes at twice the rate of the other, embedded spherulites emerge as shown in Fig. 9. This type of microstructure has been experimentally observed in isotactic polypropylene [35].

IV. CONCLUSION

In this paper we have employed a diffuse-interface modeling approach to investigate crystallization phenomena and morphological evolution in amorphously deposited organic thin films. In particular, we have demonstrated that a wide variety of microstructures can arise during the crystallization process when the fast-growing crystallographic axis is allowed to vary in three dimensions and a thermodynamic free energy is introduced to favor certain out-of-plane orientations during an effectively 2D crystal growth process. Tuning the relative thermodynamic stability of different out-of-plane orientations results in complex morphologies such as sectors and centers, while altering parameters such as the anisotropy, degree of densification, and kinetics of multiple polymorphs leads to further variations in the microstructure of the film. Transitions from an edge-on to a face-on orientation or vice versa can be driven by either kinetic or thermodynamic reasons, resulting in intriguing microstructures such as petal-shaped interfaces or radiating thin strands. Substrate patterning can produce arbitrarily shaped edge-on and face-on regions; however, feature resolution may be limited by the relative crystallization rates of different orientations as well as the amplitude of fluctuations. We have also demonstrated that interesting morphologies emerge when the thermodynamic preference of edge-on vs face-on orientations is modified during the crystallization process.

Although the development of our model has been inspired by small-molecule organic semiconductors, our findings are in principle applicable to films composed of any material with a preferred axis of crystal growth. For example, polymers are known to exhibit diverse morphologies [34,35] that closely resemble those presented in this paper. While the lamellar structure of semicrystalline polymers is not identical to the planar stacking geometry assumed in this model [36], the qualitative concepts presented here regarding the interplay between kinetics and thermodynamics as well as the manifestation of polymorphism are nevertheless relevant to polymers as well as other spherulite-forming systems. Furthermore, the extension of our model to account for additional physical phenomena may help explain certain experimentally observed morphologies and relative crystallization rates of differently oriented grains that cannot yet be reproduced by the current model. For example, here it has been assumed that films tend toward either face-on or edge-on crystallization, but films with intermediate orientations have also been experimentally observed [8,13].

It is important to note that the framework used in our model possesses both advantages and disadvantages compared to other 3D orientational diffuse-interface models in the literature, which employ quaternions [22,23] or orthogonal matrices [32] to fully describe local orientations. In these models the mobilities of the crystallinity order parameter and the orientational fields can be varied independently, allowing for a wider range of resultant morphologies by simply tuning the relative mobility values [17]. Our model lacks this degree of freedom due to its use of Cartesian coordinates for time evolution, but it instead benefits from simple nonsingular time evolution equations as well as the ability to maintain numerical stability with larger time steps. Another consequence of using a single mobility is that enforcing it to have a very low value in the crystalline phase freezes not only the orientation but also the degree of crystallinity, thereby preventing the crystalline phase from transforming to any other phase or even undergoing grain growth processes, which is clearly unphysical over extended time scales. However, in this paper we have only investigated the process of crystallization and hence this model remains valid for the applications considered. Finally, since we focus on the direction of one fast-crystallizing axis, we avoid including unnecessary additional parameters in our model by assuming that the local orientation in the plane perpendicular to $\vec{\phi}$ is constant throughout the film. However, in situations with different crystalline symmetries it may be necessary to

use quaternions to provide a more complete description of 3D orientations. In closing, we hope that the approach and findings presented in this paper provide inspiration for new experiments as well as theoretical work toward the ultimate goal of guiding experiments through the large phase space of possible thin film microstructures by better understanding the physical mechanisms controlling both nucleation and growth processes.

ACKNOWLEDGMENTS

This work was partly supported by an NSF-DMR Grant No. 0819860 (Princeton Center for Complex Materials, a Materials Research Center) and by the National Science Foundation Graduate Research Fellowship under Grant No. DGE 1148900. Useful discussions with A. Hiszpanski and Y.-L. Loo are gratefully acknowledged.

[1] G. H. Gelinck, H. E. A. Huitema, E. van Veenendaal, E. Cantatore, L. Schrijnemakers, J. B. van der Putten, T. C. Geuns, M. Beenhakkers, J. B. Giesbers, B.-H. Huisman *et al.*, Nat. Mater. **3**, 106 (2004).
[2] J. Mabeck and G. Malliaras, Anal. Bioanal. Chem. **384**, 343 (2006).
[3] Y. Lin, Y. Li, and X. Zhan, Chem. Soc. Rev. **41**, 4245 (2012).
[4] S. S. Lee, S. Muralidharan, A. R. Woll, M. A. Loth, Z. Li, J. E. Anthony, M. Haataja, and Y.-L. Loo, Chem. Mater. **24**, 2920 (2012).
[5] K. C. Dickey, J. E. Anthony, and Y.-L. Loo, Adv. Mater. **18**, 1721 (2006).
[6] S. S. Lee, S. B. Tang, D.-M. Smilgies, A. R. Woll, M. A. Loth, J. M. Mativetsky, J. E. Anthony, and Y.-L. Loo, Adv. Mater. **24**, 2692 (2012).
[7] R. J. Kline, S. D. Hudson, X. Zhang, D. J. Gundlach, A. J. Moad, O. D. Jurchescu, T. N. Jackson, S. Subramanian, J. E. Anthony, M. F. Toney, and L. J. Richter, Chem. Mater. **23**, 1194 (2011).
[8] A. M. Hiszpanski, S. S. Lee, H. Wang, A. R. Woll, C. Nuckolls, and Y.-L. Loo, ACS Nano **7**, 294 (2013).
[9] S. S. Lee and Y.-L. Loo, Annu. Rev. Chem. Biomol. Eng. **1**, 59 (2010).
[10] Z. B. Henson, K. Mullen, and G. C. Bazan, Nat. Chem. **4**, 699 (2012).
[11] J. Y. Lee, S. Roth, and Y. W. Park, Appl. Phys. Lett. **88**, 252106 (2006).
[12] S. K. Park, D. A. Mourey, S. Subramanian, J. E. Anthony, and T. N. Jackson, Appl. Phys. Lett. **93**, 043301 (2008).
[13] C. Schünemann, D. Wynands, K.-J. Eichhorn, M. Stamm, K. Leo, and M. Riede, J. Phys. Chem. C **117**, 11600 (2013).
[14] S. S. Lee, J. M. Mativetsky, M. A. Loth, J. E. Anthony, and Y.-L. Loo, ACS Nano **6**, 9879 (2012).
[15] S. S. Lee, M. A. Loth, J. E. Anthony, and Y.-L. Loo, J. Am. Chem. Soc. **134**, 5436 (2012).
[16] G. Horowitz and M. E. Hajlaoui, Adv. Mater. **12**, 1046 (2000).
[17] L. Gránásy, T. Pusztai, G. Tegze, J. A. Warren, and J. F. Douglas, Phys. Rev. E **72**, 011605 (2005).
[18] L. Gránásy, L. Rátkai, A. Szállás, B. Korbuly, G. I. Tóth, L. Krnyei, and T. Pusztai, Metall. Mater. Trans. A (to be published).
[19] A. Durr, B. Nickel, V. Sharma, U. Taffner, and H. Dosch, Thin Solid Films **503**, 127 (2006).
[20] T. Djuric, T. Ules, H.-G. Flesch, H. Plank, Q. Shen, C. Teichert, R. Resel, and M. G. Ramsey, Cryst. Growth Design **11**, 1015 (2011).
[21] H. Sirringhaus, P. Brown, R. Friend, M. Nielsen, K. Bechgaard, B. Langeveld-Voss, A. Spiering, R. A. Janssen, E. Meijer, P. Herwig, and D. M. de Leeuw, Nature (London) **401**, 685 (1999).
[22] T. Pusztai, G. Bortel, and L. Gránásy, Europhys. Lett. **71**, 131 (2005).
[23] T. Pusztai, G. Tegze, G. I. Toth, L. Kornyei, G. Bansel, Z. Fan, and L. Gránásy, J. Phys.: Condens. Matter **20**, 404205 (2008).
[24] A. Hiszpanski and Y.-L. Loo (private communication).
[25] A. M. Hiszpanski and Y.-L. Loo, Energy Environ. Sci. **7**, 592 (2014).
[26] J. Bernstein, R. J. Davey, and J.-O. Henck, Angew. Chem. Int. Ed. Engl. **38**, 3440 (1999).
[27] R. Kobayashi, Physica D **63**, 410 (1993).
[28] B. Morin, K. R. Elder, M. Sutton, and M. Grant, Phys. Rev. Lett. **75**, 2156 (1995).
[29] R. Kobayashi, J. Warren, and W. Carter, Physica D **119**, 415 (1998).
[30] S. Muralidharan, Ph.D. thesis, Princeton University, 2012.
[31] K. Aguenaou, Ph.D. thesis, McGill University, 1997.
[32] R. Kobayashi and J. A. Warren, Physica A **356**, 127 (2005).
[33] H. A. Makse, S. Havlin, M. Schwartz, and H. E. Stanley, Phys. Rev. E **53**, 5445 (1996).
[34] O. Farrance, R. Jones, and J. Hobbs, Polymer **50**, 3730 (2009).
[35] G. Schulze and H.-P. Wilbert, Colloid Polym. Sci. **267**, 108 (1989).
[36] Y.-X. Liu and E.-Q. Chen, Coord. Chem. Rev. **254**, 1011 (2010).